



Remobilization of inverted normal faults drives active extension in the axial zone of the southern Apennine mountain belt (Italy)

G. Camanni^{1,2}, G. De Landro^{3*}, S. Mazzoli⁴, M. Michele⁵, T. Muzellec³, A. Ascione¹, D. P. Schaff⁶, S. Tarantino⁷ and A. Zollo³

¹ DiSTAR, Università degli Studi di Napoli 'Federico II', Naples, Italy

² Dipartimento di Scienze Chimiche e Geologiche, Università di Modena e Reggio Emilia, Modena, Italy

³ RISSC-Lab, Dipartimento di Fisica E. Pancini, Università degli Studi di Napoli 'Federico II', Naples, Italy

⁴ School of Science and Technology – Geology Division, University of Camerino, Camerino, Italy

⁵ Istituto Nazionale di Geofisica e Vulcanologia, Rome, Italy

⁶ Lamont–Doherty Earth Observatory of Columbia University, Palisades, NY 10964, USA

⁷ Istituto Nazionale di Geofisica e Vulcanologia, L'Aquila, Italy

GC, 0000-0001-9690-2583; GDL, 0000-0003-1136-1357

* Correspondence: grazia.delandro@unina.it

Abstract: The Irpinia region is one of the most seismically active areas of Italy owing to ongoing, late-orogenic extension in the axial zone of the Apennine mountain belt. However, the 3D architecture and the nature of the faults that drive this extension are still uncertain, posing challenges to seismic hazard assessment. Here, we address these uncertainties by integrating a new catalogue of high-resolution micro-seismicity ($M_L < 3.5$) complemented by earthquake focal mechanisms, with existing 3D seismic velocity models and geological data. We found that micro-seismicity is primarily taking place along a segmented, approximately 60 km long, deep-seated, Mesozoic normal fault that was inverted during the shortening stages of the Apennine orogeny and then extensionally reactivated during the Quaternary. These findings suggest that multiple events of reactivation of long-lived faults can weaken their strength, making them prone to co-seismic remobilization under newly imposed strain fields in active mountain belts.

Supplementary material: A supplementary information file and table are available at <https://doi.org/10.6084/m9.figshare.c.7401635>

Received 6 September 2024; **revised** 14 November 2024; **accepted** 19 November 2024

The Irpinia region, located in the axial zone of the Neogene southern Apennines mountain belt (e.g. Ippolito *et al.* 1975; Roure *et al.* 1991; Cello and Mazzoli 1999; Pescatore *et al.* 1999; Menardi Noguera and Rea 2000; Patacca and Scandone 2007; Ciarcia and Vitale 2024), is one of the most seismically active areas of Italy, owing to continuing, late-orogenic extension ($c. 3 \text{ mm a}^{-1}$, D'Agostino 2014; e.g. Ascione *et al.* 2013 and references therein). In 1980, the Irpinia region was struck by an M_s 6.9 earthquake (the largest Italian event in the last 100 years) that originated from a complex multi-segment rupture process (e.g. Bernard and Zollo 1989) and caused severe damage and thousands of fatalities in a wide epicentral area. During the last four decades, a moderate aftershock and background seismicity has continuously affected the crustal volume delimited by the faults that were activated during the 1980 M_s 6.9 Irpinia earthquake (e.g. De Matteis *et al.* 2012; Amoroso *et al.* 2014). Furthermore, since 2005, the monitoring of the Irpinia region by dense seismic networks (Irpinia Seismic Network (ISNet) and the Istituto Nazionale di Geofisica e Vulcanologia network (INGV)) revealed the occurrence of persistent seismicity with magnitude near zero (De Landro *et al.* 2015; Amoroso *et al.* 2017; D'Agostino *et al.* 2018; Picozzi *et al.* 2019; Festa *et al.* 2021; Palo *et al.* 2023a, b; Scotto di Uccio *et al.* 2024; Tarantino *et al.* 2024).

However, the 3D architecture and the nature of the faults that are being remobilized nowadays, which may control this seismicity and drive the continuing extension, are not yet well understood. These uncertainties pose significant challenges for seismic hazard assessment in this highly active and densely populated region of

southern Italy. In this work, we address these uncertainties by the integrated analysis of a newly reconstructed, high-resolution catalogue of approximately 15 years of micro-seismicity ($M_L < 3.5$) complemented by newly calculated and compiled earthquake focal mechanisms, with existing 3D seismic velocity models (De Landro *et al.* 2022) and available geological models based on surface geology and seismic interpretation (e.g. Ascione *et al.* 2013, 2020).

Geological structure and evolution of the axial zone of the southern Apennines

The architecture of the axial zone of the southern Apennines is characterized by a two-layer structure (Mazzoli *et al.* 2014; Fig. 1). The upper layer consists of a far-travelled (>50 km) allochthonous assemblage forming an intensely deformed, thin-skinned fold and thrust belt. This overlies a less deformed, thick-skinned lower layer. The thin-skinned belt primarily involves Mesozoic–Cenozoic successions of the Apennine Platform (shallow-water carbonates) and of the Lagonegro Basin (shallow-water to pelagic limestones, radiolarian cherts and shales). Conversely, the deeper thick-skinned belt involves the 6–8 km thick shallow-water carbonate succession of the Apulian Platform, as well as the Lower Triassic siliciclastic deposits located at its base and the underlying basement. The recent tectonic emplacement of the thin-skinned belt is indicated by the occurrence, in its footwall, of Pliocene to Lower Pleistocene foreland basin deposits resting on top of the Apulian Platform carbonates and penetrated by numerous oil wells (Mazzoli *et al.*

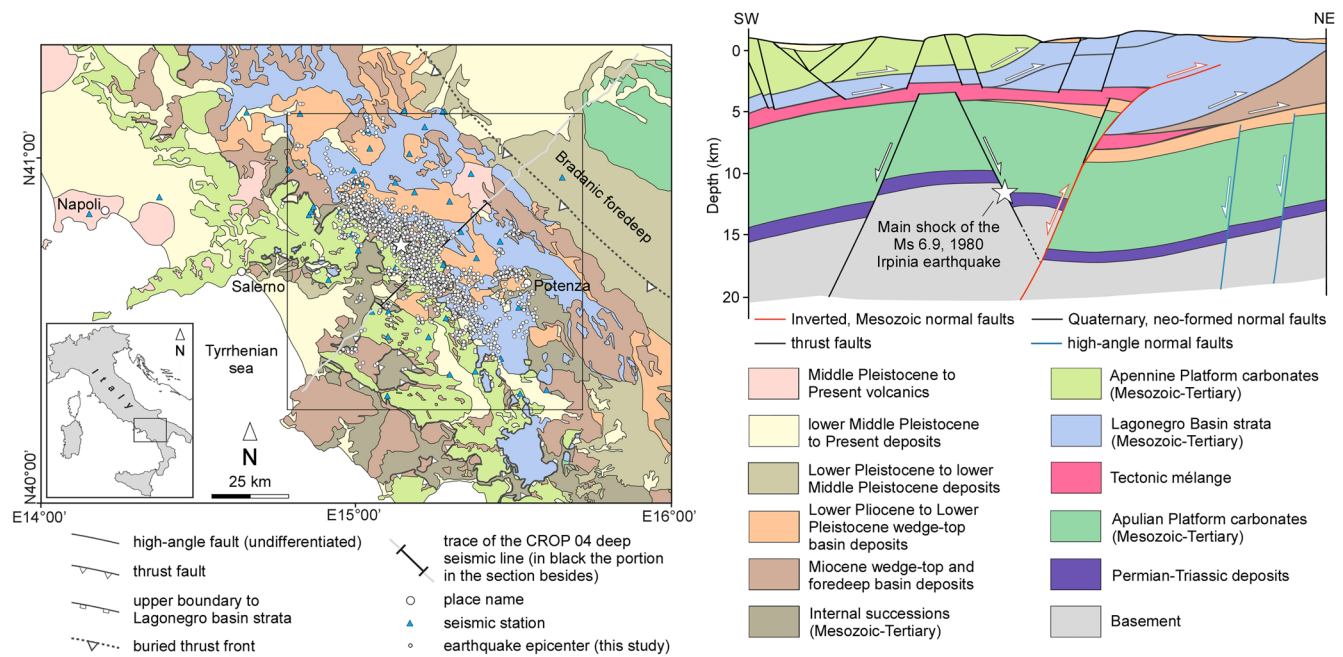


Fig. 1. Geological setting of the study area in the southern Apennines mountain belt. It should be noted that the Quaternary, neo-formed normal faults are shown only in the section. The box in the map corresponds to the map area of Figure 2a. Source: modified after Ascione *et al.* (2020); the section is based on the integration of surface geological data with subsurface constraints provided by the CROP 04 deep seismic reflection profile (Mazzotti *et al.* 2007) calibrated with oil-well logs (Patacca 2007).

2001). Since the middle Pleistocene the axial zone of the southern Apennines has been undergoing a phase of late-orogenic extension (Cello *et al.* 1982; Cinque *et al.* 1993; Hippolyte *et al.* 1994; Butler *et al.* 2004; Caiazza *et al.* 2006). This extension led to the development of neo-formed Quaternary extensional faults that dissect the mountain belt (black faults in the section of Fig. 1) and is responsible for the continuing seismicity within the study area.

Importantly for this work, the thick-skinned belt (where the seismicity is mostly focused) is composed of deep-seated, steeply dipping reverse faults mainly formed by the reverse- or oblique-slip reactivation ('inversion') of pre-existing Mesozoic normal faults (Mazzoli *et al.* 2000, 2008; Butler *et al.* 2004; Shiner *et al.* 2004; Ascione *et al.* 2013, 2020; Amoroso *et al.* 2014, 2017). These structures control the so-called Apulian inversion belt (Mazzoli *et al.* 2008). The inversion tectonics model for the Apulian Platform shortening-related structures was derived by the interpretation of high-resolution seismic reflection profiles calibrated with numerous oil wells and subsequent depth conversion, cross-section balancing and restoration (e.g. Shiner *et al.* 2004). Shortening-related reactivation of inherited faults in the Apulian Platform carbonates was unravelled by the interpretation of high-quality seismic data also in the outer zone of the southern Apennines by Bitonte *et al.* (2021). The latter researchers also documented fault propagation into the foreland basin deposits as a result of such fault reactivation. Within the study area, the development of the Apulian inversion belt was controlled by the reverse- or oblique-slip reactivation of a SW-dipping Mesozoic normal fault (red fault in the cross-section of Fig. 1). This structure produced a prominent uplift of the Apulian Platform carbonates in its hanging wall (Ascione *et al.* 2013, 2020). The carbonate culmination is dissected by a deeply rooted Quaternary horst, the NW-dipping boundary fault of which was associated with the M_s 6.9 main shock of the 1980 Irpinia earthquake (Ascione *et al.* 2013, 2020; Amoroso *et al.* 2014).

Seismological data and methods

The micro-seismicity catalogue on which this work is based was obtained by analysing a dataset consisting of about 2400 micro-

earthquakes, with local magnitude (M_L) ranging between 0.5 and 3.2. These events were recorded by 42 ISNet and INGV stations from August 2005 to December 2022. We used manually picked first P- and S-wave arrival times from the ISNet bulletin (<http://isnet-bulletin.fisica.unina.it/cgi-bin/isnet-events/isnet.cgi>) and integrated manually picks from INGV stations (see Supplementary material SM1). Initially, we located the events with a probabilistic method (NLLoc, Lomax *et al.* 2009) and a 3D velocity model optimized for the area (De Landro *et al.* 2022), which allowed us to obtain a first location catalogue with an average RMS residual of 0.15 s and horizontal location errors within 1.5 km (average 800 m) and vertical location errors within 2 km (average 1.2 km) for 85% of events. Successively, we refined the absolute 3D location with the double-difference approach (HypoDD, Michele *et al.* 2019; Waldhauser and Ellsworth 2000) by using catalogue (CT) and cross-correlation (CC) differential times (Schaff and Waldhauser 2005). The final residual RMS was 0.008 s for CC data and 0.03 s for CT data. The final horizontal and vertical location errors were within 100 m for most of the events. For further details on the location strategy and method used see Supplementary material MS2. The final dataset is available in the catalogue of De Landro (2024).

As a further constraint on the fault geometry and kinematics, the composite focal mechanisms of significant clusters of this new micro-seismicity catalogue were also calculated using the consolidated code PPFIT (Reasenber and Oppenheimer 1985). Similarly to Festa *et al.* (2021) and Muzellec *et al.* (2024), we evaluated, for four selected hypocentre clusters, the composite focal mechanisms (red 'beach balls' in Fig. 2) by integrating the polarities of co-located events for the construction of more constrained mechanisms. Furthermore, where it was not possible to calculate composite focal mechanisms owing to the lack of hypocentre clusters, we integrated four additional focal mechanisms of single events (dark grey 'beach balls' in Fig. 2). These were selected among the focal mechanisms available from the ISNet bulletin and refined by using the 3D location. To validate this selection, we compared these mechanisms with those obtained by De Matteis *et al.* (2012), in which the author performed an extensive analysis of focal mechanisms and refined the stress field of the Irpinia region.

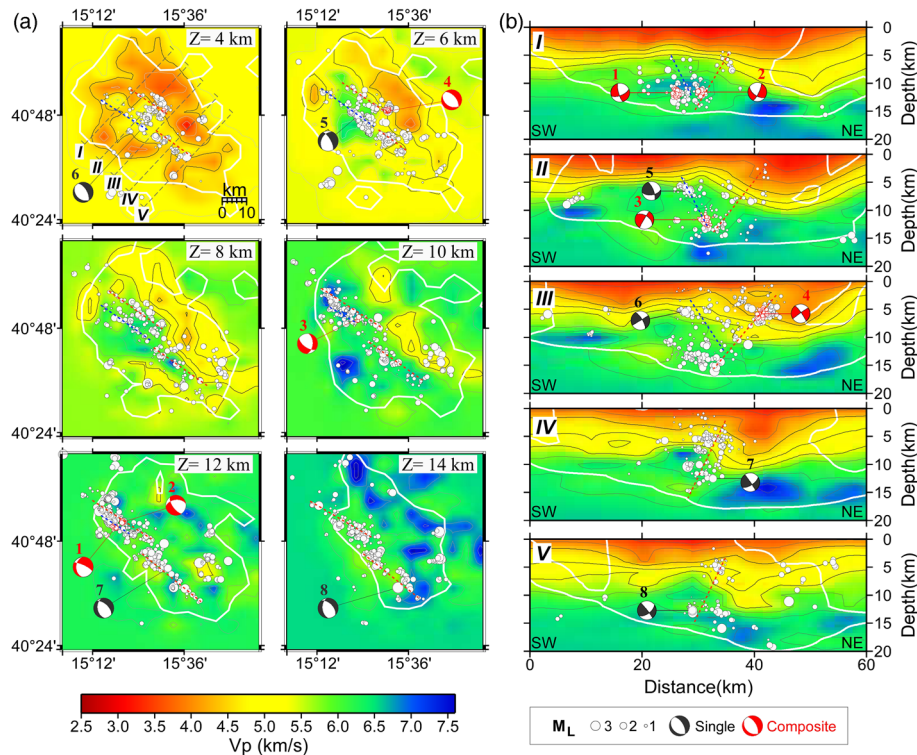


Fig. 2. Horizontal (a) and vertical (b) sections through the P-wave velocity model and earthquake hypocentres (this study) within the Irpinia region. Earthquake hypocentres (shown as white dots) are projected within ± 1 km and within ± 2 km on either side of the horizontal and vertical sections, respectively. The dimension of hypocentres is related to the local magnitude, as indicated in the legend. The P-wave isovelocity contours are displayed every 0.5 km s^{-1} and the thicker ones correspond to the 4.5 , 5 and 5.5 km s^{-1} contours. The white line indicates the boundary of resolution of the P-wave velocity model. Locations of the vertical sections in (b) are indicated in the 4 km horizontal section in (a). Focal mechanisms of event clusters (i.e. composite focal mechanisms; red ‘beach ball’) and single events (dark grey ‘beach ball’), numbered following the NW–SE direction, are plotted using a lower hemisphere projection in (a) and along vertical planes parallel to the sections in (b). The dashed red and blue lines are traced approximately through the middle and parallel to the long axis of the wide SW- and NE-dipping hypocentre clusters, respectively. Source: P-wave velocity model from De Landro *et al.* (2022).

(For further details on focal mechanism data, calculation, evaluation and selection, and uncertainties see [Supplementary material SM3](#) and [Table SM3](#) and De Landro (2024).)

As a constraint on the depth and geometry of the top of the Apulian Platform carbonates, we used the 3D P-wave velocity model of De Landro *et al.* (2022). This model was built using a linearized, tomographic approach in which about 13 000 P- and S-wave arrival times were inverted to retrieve, jointly, the location of about 1500 earthquakes of the ISNet catalogue and the P- and S-phase velocity parameters. Similarly to Amoroso *et al.* (2014, 2017), a multi-scale strategy was applied, starting from a coarser parameterization to a finer one of $3 \times 3 \times 1 \text{ km}^3$, with a forward grid of 500 m step size. The model resolution was assessed by the integration of the resolution matrix, composed by intrinsic resolution and spreading function, and the ray density around each node.

Spatial distribution of micro-seismicity and P-wave velocities

Earthquake hypocentres within the study area mostly extend from about 3 to 14 km depth and are generally distributed along an about 20 km wide, 60 km long, NW–SE-elongated belt (Figs 1 and 2). Within this distribution, distinct features can be recognized from horizontal and vertical sections through the data.

On horizontal sections (Fig. 2a), from approximately 10 km depth and downward, hypocentres are roughly aligned along two NW–SE-elongated clusters, each $c. 5\text{--}10 \text{ km}$ wide and $c. 30 \text{ km}$ long (see red dashed lines in Fig. 2a). These two clusters are arranged in a geometry in which a SE cluster steps northwestward to the right into a NW cluster, the latter being associated with the

largest concentration of hypocentres. Notably, at all depths, the volume in which this step occurs is characterized by a decreased density of hypocentres. From approximately 8 km depth and upwards, these two clusters become shorter and less clearly defined, whereas another NW–SE-elongated cluster more prominently emerges located to the SW of the NW cluster. This other cluster is $c. 5\text{--}10 \text{ km}$ wide and 30 km long, being best identifiable on the 8 and 6 km depth horizontal sections (see blue dashed lines in Fig. 2a).

On vertical sections perpendicular to the NW–SE map-view clusters (i.e. NE–SW; Fig. 2b), earthquake hypocentres forming the two major, right-stepping map-view clusters overall align into a primary, locally discontinuous, SW-dipping cluster $c. 5\text{--}10 \text{ km}$ wide, recognizable throughout the study area (see red dashed lines in Fig. 2b). This cluster widens upwards near the centre of the study area (section III in Fig. 2b). In contrast, the shallower NW–SE-elongated cluster in the NE sector of the study area corresponds to a NW-dipping, $c. 5\text{--}10 \text{ km}$ wide cluster in cross-section (see blue dashed lines in Fig. 2b).

From approximately 10 km depth upwards on horizontal sections, the two major NW–SE-elongated hypocentre clusters roughly coincide with a distinct NW–SE boundary in the P-wave velocity model, between higher velocities in the SW and lower velocities in the NE (Fig. 2a). In all vertical sections, this feature manifests as a prominent deepening of low P-wave velocities from SW to NW (Fig. 2b). This is best highlighted by the 4.5 , 5 and 5.5 km s^{-1} isovelocity contours and approximately occurs across the primary SW-dipping cluster of hypocentres (Fig. 2b). It is worth noting that this deepening is largest in the central and northwestern parts of the study area (Fig. 2).

In the 10, 8 and 6 km depth sections (Fig. 2a), the boundary between higher and lower velocities shows a curved morphology in map view, taking on a more north–south orientation at the location of the step between the two deep NW–SE-elongated hypocentre clusters. This curved deepening of low velocities is clearly depicted by the 5.5 km s^{-1} isovelocity surface (Fig. 3).

Earthquake focal mechanisms

The four composite and the four compiled single event earthquake focal mechanisms within the study area all display an approximately pure dip-slip, extensional kinematics (Fig. 2a and b; see also De Landro 2024 and Supplementary material Table SM3), in agreement with the regional strain field of the study area (De Matteis *et al.* 2012; Bello *et al.* 2021; Festa *et al.* 2021; Ricigliano Eqk report, RISSC-Lab 2024). In general, each focal mechanism has nodal planes striking roughly NW–SE sub-parallel to the overall orientation of the earthquake hypocentre clusters, although minor variations to these orientations exist. For example, some focal mechanisms include an approximately north–south-oriented nodal plane (e.g. focal mechanisms 1, 3, 5, 7 and 8, Fig. 2a), whereas others include an approximately east–west-oriented nodal plane (e.g. focal mechanism 2, Fig. 2a). Dip angles of the focal mechanism nodal planes are also overall consistent with the dip of the main earthquake hypocentre clusters (i.e. either SW- or NE-dipping; Fig. 2b). However, whereas some focal mechanisms are associated with two moderately dipping nodal planes (e.g. focal mechanisms 2, 3, 7 and 8, Fig. 2b), others display a pair of nodal planes in which one is steeply dipping and the other is gently dipping (focal mechanisms 1, 4, 5 and 6, Fig. 2b).

Discussion and conclusions

As we have seen, the deep geological structure within the study area is that of an Apulian Platform carbonates culmination bounded to the NE by, and uplifted along, an inverted Mesozoic normal fault (cross-section in Fig. 1). When integrating the seismological data presented above with this geological information, several coherent features become apparent (Fig. 4). In particular, (1) the shallow high

P-wave velocities nearly coincide with the uplifted Apulian Platform carbonates and (2) the primary SW-dipping cluster of hypocentres approximately aligns with the inverted Mesozoic normal fault (red fault in the section of Fig. 1) responsible for this uplift. Because both seismological features are recognizable throughout the study area, we infer that a structural model in which Apulian Platform carbonates are uplifted along an inverted SW-dipping Mesozoic normal fault holds for the entire study area (Fig. 4). Furthermore, considering that both earthquake hypocentres and P-wave velocities are right-stepped (Figs 2 and 3), the inverted fault may be confidently interpreted as also stepped in map view (Fig. 4). This is further supported by results of gravity data modelling (Improta *et al.* 2003; see also De Landro *et al.* 2015), which show that the depocentre ahead of the inverted fault is also right-stepped in map view. This feature most probably reflects the original segmentation of the precursor normal fault, which comprised two fault segments separated by a relay zone (e.g. Camanni *et al.* 2023, and references therein).

The inverted Mesozoic normal fault coincides both in map view and in cross-section with an approximately 5–10 km wide zone of earthquake hypocentres (Figs 2 and 4), rather than with a well-delineated feature. We interpret this as due to the combined effect of this structure probably being a broad fault zone (a common feature for faults; e.g. Childs *et al.* 2009) rather than an individual fault surface (see also De Matteis *et al.* 2012 for a similar interpretation of the micro-seismicity in the Irpinia region) and of the uncertainty in the event's location. However, the overall dip and strike of the fault zone are consistent with those of the nodal planes of the focal mechanisms (i.e. NW–SE striking and SW-dipping, Fig. 4).

For the northern part of the study area (i.e. north of the step of the inverted fault), the attitude of the faults included in this new structural model (Fig. 4) is consistent with that derived from the 0 and 40 s sub-events of the 1980 Irpinia earthquake (Westaway and Jackson 1984; Bernard and Zollo 1989; Pantosti and Valensise 1990; Pingue *et al.* 1993; Amoroso *et al.* 2005, 2011). On the other hand, for the southern part of the study area this new structural model is consistent with the minority interpretation provided by Amoroso *et al.* (2005, 2011) for the 20 s sub-event (which most researchers interpreted to have occurred along a NE-dipping fault, in some case interpreted to be low angle; e.g. Bernard and Zollo 1989).

The micro-seismicity within the study area is associated with continuing late-orogenic extension, in agreement with focal mechanisms that display normal sense kinematics (e.g. this study; De Matteis *et al.* 2012; Festa *et al.* 2021; Fig. 4). This may appear counterintuitive, as we found that most seismicity is taking place along an inverted fault that preserves its reverse net displacement associated with the uplift of Apulian Platform carbonates (Figs 1 and 4). This fault is long-lived and has been active with a normal sense of movement in the Mesozoic and reactivated with a reverse- or oblique-slip kinematics during the Apennine orogeny. We suggest that these multiple slip events weakened the strength of the fault, making it prone to further remobilization ('negative inversion') under the newly imposed extensional strain field affecting the Irpinia region. Whereas in the SE part of the study area this is the only fault driving continuing extension, in the NW sector this fault is acting in association with two further neo-formed faults that define a Quaternary horst within the Apulian Platform carbonates (one of these two faults, i.e. the NE dipping one, generated the M_s 6.9 main shock of the 1980 Irpinia earthquake and contains most of the micro-seismicity; Fig. 4). This occurs in a sector where the net displacement of the inverted fault is maximum, as shown by the highest deepening of P-wave velocities that define the deepest top Apulian Platform carbonates in the fault footwall; Fig. 2). Based on this observation, we suggest that the need for extensional readjustment is most pronounced in this sector, thus requiring the involvement of all three faults.

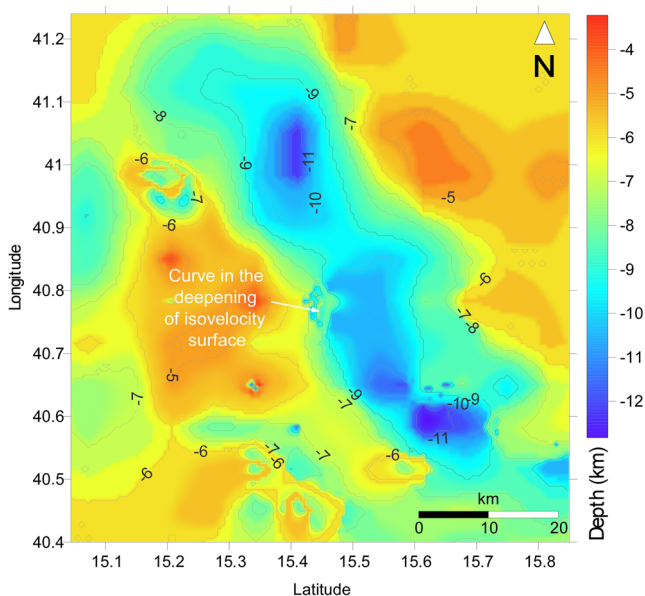


Fig. 3. The 5.5 km s^{-1} isovelocity surface of the P-wave velocity model within the study area. It should be noted that low P-wave velocity material deepens from SW to NE, and that this takes place along a curved interface. Source: P-wave velocity model from De Landro *et al.* (2022).

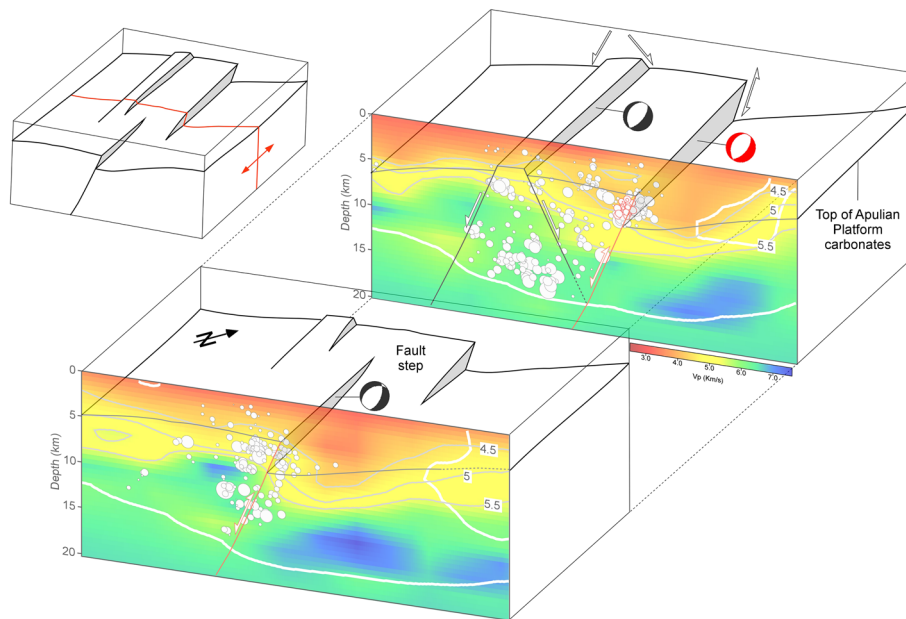


Fig. 4. A 3D block diagram of the central part of the study area built by integrating the new micro-seismicity catalogue of this work with P-wave velocity and available geological data. The diagram comprises two portions displaced for visualization purposes (complete block diagram in the upper left corner). The location of the top vertical section through the middle of the diagram coincides with that of the geological cross-section in Figure 1 and with that of section III of Figure 2b, whereas the bottom section corresponds to the SE side of the block diagram and coincides with section IV of Figure 2b. Earthquake hypocentres (shown as white dots) are projected from 2 km on either side of the vertical sections. Focal mechanisms correspond to 4, 6 and 7 in Figure 2a, seen in map view. Source: P-wave velocity from De Landro *et al.* (2022); geological data from Ascione *et al.* (2013, 2020).

These findings have broader implications for other active mountain belts characterized by a thick-skinned style of deformation and inversion tectonics (e.g. Taiwan: Lacombe and Mouthereau 2002; Camanni *et al.* 2014, 2016; Western Alps: Mosar 1999; Zagros: Tavani *et al.* 2020). When assessing seismic hazard in such mountain belts, particular attention should be directed towards long-lived faults. The results of this work also indicate that this should be done regardless of the consistency between the geological displacement of the fault and the kinematics of the newly imposed strain field.

Scientific editing by Francesca Remitti

Acknowledgements We thank the Irpinia Near Fault Observatory revision team that works on the INFO bulletin construction (<http://isnet-bulletin.fisica.unina.it/cgi-bin/isnet-events/isnet.cgi>). The code FPFIT (Reasenber and Oppenheimer 1985) was used for calculating the composite focal mechanisms. The Generic Mapping Tools (GMT) version 4 (Wessel *et al.* 2019), licensed under LGPL version 3 or later and available at <https://www.generic-mapping-tools.org/>, were used to produce some of the figures. Two anonymous reviewers and the *Journal of the Geological Society* editors are also acknowledged.

Author contributions GC: conceptualization (lead), data curation (equal), formal analysis (equal), investigation (equal), methodology (equal), software (equal), supervision (equal), validation (equal), visualization (equal), writing – original draft (lead); GDL: conceptualization (equal), data curation (equal), formal analysis (lead), funding acquisition (equal), investigation (equal), methodology (equal), project administration (equal), resources (equal), software (equal), supervision (equal), validation (equal), visualization (equal), writing – review & editing (lead); SM: conceptualization (supporting), investigation (equal), validation (equal), writing – review & editing (equal); MM: data curation (supporting), formal analysis (equal), investigation (supporting), software (supporting); TM: data curation (supporting), formal analysis (equal), investigation (supporting), software (supporting), writing – review & editing (supporting); AA: conceptualization (supporting), formal analysis (supporting), investigation (supporting), writing – review & editing (supporting); DPS: data curation (supporting), formal analysis (equal), investigation (supporting), software (supporting), writing – review & editing (supporting); ST: data curation (supporting), formal analysis (equal), investigation (supporting), software (supporting), writing – review & editing (supporting); AZ: conceptualization (supporting), funding acquisition (equal), investigation (equal), project administration (equal), resources (equal), supervision (equal), validation (equal), writing – review & editing (equal).

Funding The authors acknowledge financial support from the Project TRHAM, ‘Relation Between 3D Thermo-Rheological Model And Seismic Hazard For The Risk Mitigation In The Urban Areas Of Southern Italy’ funded by the European Union, Next Generation EU, Mission 4, Component 2, CUP

B53D23033710001 (Grant Number P2022P37SN); and from the Project FRACTURES, ‘Multiscale study of seismogenic processes in Campania–Lucania Apennines using machine learning algorithms and multiparametric observations’ funded by the European Union, Next Generation EU, Mission 4, Component 2, CUP B53D23006980006 (Grant Number 2022BEKFN2). The work of A.Z. was supported in part by Project ‘PE0000005–RETURN-SPOKE 3-CUP UNINA: E63C220002000002’.

Competing interests The authors declare that they have no known competing financial interests or personal relationships that could have appeared to influence the work reported in this paper.

Data availability The micro-seismicity catalogue and the focal mechanisms used in this study are stored in the following repository under the CC BY 4.0 licence: <https://zenodo.org/records/11208080> (De Landro 2024). The 3D P-wave velocity model used in this study is available in the following repository under the CC BY 4.0 licence: <https://doi.org/10.5281/zenodo.14637925>. This study used the Irpinia Near Fault Observatory (<https://isnet.unina.it>) data and products. Seismic data are available at the EIDA website (<https://eida.ingv.it/>) and at the EPOS Data Portal (<https://www.epos-eu.org/dataportal>), IRPINIA Seismic Velocity and Acceleration Waveforms (Continuous) provided by Università di Napoli Federico II and INGV, networks IX and IV. The seismic bulletin catalogue is available at the Irpinia Near Fault Observatory website (<http://isnet-bulletin.fisica.unina.it/cgi-bin/isnet-events/isnet.cgi>) and at the EPOS Data Portal (<https://www.epos-eu.org/dataportal>), IRPINIA Seismic Events provided by Università di Napoli Federico II.

References

- Amoroso, O., Ascione, A., Mazzoli, S., Virieux, J. and Zollo, A. 2014. Seismic imaging of a fluid storage in the actively extending Apennine mountain belt, southern Italy. *Geophysical Research Letters*, **41**, 3802–3809, <https://doi.org/10.1002/2014GL060070>
- Amoroso, O., Russo, G. *et al.* 2017. From Velocity and Attenuation Tomographies to Rock Physical Modeling: inferences on fluid-driven earthquake processes at the Irpinia fault system in Southern Italy. *Geophysical Research Letters*, **44**, 6752–6760, <https://doi.org/10.1002/2016GL072346>
- Amoroso, A., Crescentini, L. and Scarpa, R. 2005. Faulting geometry for the complex 1980 Campania–Lucania earthquake from levelling data. *Geophysical Journal International*, **162**, 156–168, <https://doi.org/10.1111/j.1365-246X.2005.02652.x>
- Amoroso, A., Crescentini, L., Di Lieto, B. and Scarpa, R. 2011. Faulting mechanism of the Campania–Lucania 1980 earthquake, Italy, from high-resolution, 3D velocity structure, aftershock relocation, fault-plane solutions, and post-seismic deformation modeling. *Annals of Geophysics*, **54**, 806–821, <https://doi.org/10.4401/ag-4984>
- Ascione, A., Mazzoli, S., Petrosino, P. and Valente, E. 2013. A decoupled kinematic model for active normal faults: insights from the 1980, $M_s = 6.9$ Irpinia earthquake, southern Italy. *Geological Society of America Bulletin*, **125**, 1239–1259, <https://doi.org/10.1130/B30814.1>

- Ascione, A., Nardò, S. and Mazzoli, S. 2020. The MS 6.9, 1980 Irpinia Earthquake from the Basement to the Surface: a review of tectonic geomorphology and geophysical constraints, and new data on post-seismic deformation. *Geosciences*, **10**, 493, <https://doi.org/10.3390/geosciences10120493>
- Bello, S., de Nardis, R. *et al.* 2021. Fault pattern and seismotectonic style of the Campania–Lucania 1980 earthquake (Mw 6.9, Southern Italy): new multidisciplinary constraints. *Frontiers in Earth Science*, **8**, <https://doi.org/10.3389/feart.2020.608063>
- Bernard, P. and Zollo, A. 1989. The Irpinia (Italy) 1980 earthquake: detailed analysis of a complex normal faulting. *Journal of Geophysical Research*, **94**, 1631–1647, <https://doi.org/10.1029/jb094ib02p01631>
- Bitonte, R., Livio, F.A. *et al.* 2021. Frontal accretion vs. foreland plate deformation: discriminating the style of post-collisional shortening in the Apennines. *Journal of Structural Geology*, **145**, 104290, <https://doi.org/10.1016/j.jsg.2021.104290>
- Butler, R.W.H., Mazzoli, S. *et al.* 2004. Applying thick-skinned tectonic models to the Apennine thrust belt of Italy: limitations and implications. *AAPG, Memoirs*, **82**, 647–667, <https://doi.org/10.1306/M82813C34>
- Caiazzo, C., Ascione, A. and Cinque, A. 2006. Late Tertiary–Quaternary tectonics of the southern Apennines (Italy): new evidences from the Tyrrhenian slope. *Tectonophysics*, **421**, 23–51, <https://doi.org/10.1016/j.tecto.2006.04.011>
- Camanni, G., Chen, C.-H. *et al.* 2014. Basin inversion in central Taiwan and its importance for seismic hazard. *Geology*, **42**, 147–150, <https://doi.org/10.1130/G35102.1>
- Camanni, G., Alvarez-Marron, J., Brown, D., Ayala, C., Wu, Y.-M. and Hsieh, H.-H. 2016. The deep structure of south–central Taiwan illuminated by seismic tomography and earthquake hypocentre data. *Tectonophysics*, **679**, 235–245, <https://doi.org/10.1016/j.tecto.2015.09.016>
- Camanni, G., Freda, G., Delogkos, E., Nicol, A. and Childs, C. 2023. 3D geometry and displacement transfer of an oblique relay zone on outcropping normal faults. *Journal of Structural Geology*, **177**, <https://doi.org/10.1016/j.jsg.2023.105001>
- Cello, G. and Mazzoli, S. 1999. Apennine tectonics in southern Italy: a review. *Journal of Geodynamics*, **27**, 191–211, [https://doi.org/10.1016/S0264-3707\(97\)00072-0](https://doi.org/10.1016/S0264-3707(97)00072-0)
- Cello, G., Guerra, I., Tortorici, L., Turco, E. and Scarpa, R. 1982. Geometry of the neotectonic stress field in southern Italy: geological and seismological evidence. *Journal of Structural Geology*, **4**, 385–393, [https://doi.org/10.1016/0191-8141\(82\)90030-X](https://doi.org/10.1016/0191-8141(82)90030-X)
- Childs, C., Manzocchi, T., Walsh, J.J., Bonson, C.G., Nicol, A. and Schöpfer, M.P.J. 2009. A geometric model of fault zone and fault rock thickness variations. *Journal of Structural Geology*, **31**, 117–127, <https://doi.org/10.1016/j.jsg.2008.08.009>
- Ciarcia, S. and Vitale, S. 2024. Orogenic evolution of the northern Calabria–southern Apennines system in the framework of the Alpine chains in the central–western Mediterranean area. *Geological Society of America Bulletin*, <https://doi.org/10.1130/B37474.1>
- Cinque, A., Patacca, E., Scandone, P. and Tozzi, M. 1993. Quaternary kinematic evolution of the southern Apennines. Relationships between surface geological features and deep lithospheric structures. *Annals of Geophysics*, **36**, 249–260, <https://doi.org/10.4401/ag-4283>
- D’Agostino, N. 2014. Complete seismic release of tectonic strain and earthquake recurrence in the Apennines (Italy). *Geophysical Research Letters*, **41**, 1155–1162, <https://doi.org/10.1002/2014GL059230>
- D’Agostino, N., Silverii, F., Amoroso, O., Convertito, V., Fiorillo, F., Ventafredda, G. and Zollo, A. 2018. Crustal deformation and seismicity modulated by groundwater recharge of karst aquifers. *Geophysical Research Letters*, **45**, 12–253, <https://doi.org/10.1029/2018GL079794>
- De Landro, G. 2024. *Catalog of 3D DD Locations of the Irpinia Micro-Seismicity from 2008 to 2022*. Zenodo, <https://doi.org/10.5281/zenodo.11208080>
- De Landro, G., Amoroso, O., Stabile, T.A., Matrullo, E., Lomax, A. and Zollo, A. 2015. High-precision differential earthquake location in 3-D models: evidence for a rheological barrier controlling the microseismicity at the Irpinia fault zone in southern Apennines. *Geophysical Journal International*, **203**, 1821–1831, <https://doi.org/10.1093/gji/ggv397>
- De Landro, G., Amoroso, O., Russo, G., D’Agostino, N., Esposito, R., Emolo, A. and Zollo, A. 2022. Decade-long monitoring of seismic velocity changes at the Irpinia fault system (southern Italy) reveals pore pressure pulsations. *Scientific Reports*, **12**, <https://doi.org/10.1038/s41598-022-05365-x>
- De Matteis, R., Matrullo, E., Rivera, L., Stabile, T.A., Pasquale, G. and Zollo, A. 2012. Fault delineation and regional stress direction from the analysis of background microseismicity in the southern Apennines, Italy. *Bulletin of the Seismological Society of America*, **102**, 1899–1907, <https://doi.org/10.1785/0120110225>
- Festa, G., Adinolfi, G.M. *et al.* 2021. Insights into mechanical properties of the 1980 Irpinia fault system from the analysis of a seismic sequence. *Geosciences*, **11**, <https://doi.org/10.3390/geosciences11010028>
- Hippolyte, J.-C., Angelier, J. and Roure, F. 1994. A major geodynamic change revealed by Quaternary stress patterns in the southern Apennines (Italy). *Tectonophysics*, **230**, 199–210, [https://doi.org/10.1016/0040-1951\(94\)90135-X](https://doi.org/10.1016/0040-1951(94)90135-X)
- Improta, L., Bonagura, M., Capuano, P. and Iannaccone, G. 2003. An integrated geophysical investigation of the upper crust in the epicentral area of the 1980, Ms = 6.9, Irpinia earthquake (Southern Italy). *Tectonophysics*, **361**, 139–169, [https://doi.org/10.1016/S0040-1951\(02\)00588-7](https://doi.org/10.1016/S0040-1951(02)00588-7)
- Ippolito, F., D’Argenio, B., Pescatore, T. and Scandone, P. 1975. Structural–stratigraphic units and tectonic framework of southern Apennines. In: Squyres, C. (ed.) *Geology of Italy*. Libyan Society of Earth Science, Libyan Arab Republic, 317–328.
- Lacombe, O. and Mouthereau, F. 2002. Basement-involved shortening and deep detachment tectonics in forelands of orogens: insights from recent collision belts (Taiwan, western Alps, Pyrenees). *Tectonics*, **21**, 1030, <https://doi.org/10.1029/2001TC901018>
- Lomax, A., Michelini, A., Curtis, A. and Meyers, R.A. 2009. Earthquake location, direct, global-search methods. *Encyclopedia of Complexity and Systems Science*, **5**, 2449–2473, https://doi.org/10.1007/978-0-387-30440-3_150
- Mazzoli, S., Corrado, S. *et al.* 2000. Time and space variability of ‘thin-skinned’ and ‘thick-skinned’ thrust tectonics in the Apennines (Italy). *Rendiconti dell’Accademia dei Lincei, Scienze Fisiche e Naturali, Serie 9*, **11**, 5–39, <https://doi.org/10.1007/BF02904594>
- Mazzoli, S., Barkham, S., Cello, G., Gambini, R., Mattioni, L., Shiner, P. and Tondi, E. 2001. Reconstruction of continental margin architecture deformed by the contraction of the Lagonegro Basin, southern Apennines, Italy. *Journal of the Geological Society, London*, **158**, 309–319, <https://doi.org/10.1144/jgs.158.2.309>
- Mazzoli, S., D’Errico, M., Aldega, L., Corrado, S., Invernizzi, C., Shiner, P. and Zattin, M. 2008. Tectonic burial and ‘young’ (<10 Ma) exhumation in the southern Apennines fold and thrust belt (Italy). *Geology*, **36**, 243–246, <https://doi.org/10.1130/G24344A.1>
- Mazzoli, S., Ascione, A., Buscher, J.T., Pignalosa, A., Valente, E. and Zattin, M. 2014. Low-angle normal faulting and focused exhumation associated with late Pliocene change in tectonic style in the southern Apennines (Italy). *Tectonics*, **33**, <https://doi.org/10.1002/2014TC003608>
- Mazzotti, A., Stucchi, E., Fradelizio, G.L., Zanzi, L. and Scandone, P. 2007. Re-processing of the CROP-04 seismic data. *Bollettino della Società Geologica Italiana*, **7**, 141–153.
- Menardi Noguera, A. and Rea, G. 2000. Deep structure of the Campanian–Lucanian Arc (southern Apennine, Italy). *Tectonophysics*, **324**, 239–265, [https://doi.org/10.1016/S0040-1951\(00\)00137-2](https://doi.org/10.1016/S0040-1951(00)00137-2)
- Michele, M., Chiaraluce, L., Di Stefano, R. and Waldhauser, F. 2019. Fine-scale structure of the 2016–2017 Central Italy seismic sequence from data recorded at the Italian National Network. *Journal of Geophysical Research: Solid Earth*, **125**, <https://doi.org/10.1029/2019JB018440>
- Mosar, J. 1999. Present-day and future underplating in the western Swiss Alps: reconciliation of basement/wrench-faulting and thrust detachment folding of the Jura and Molasse basin in the Alpine foreland. *Earth and Planetary Science Letters*, **173**, 143–155, [https://doi.org/10.1016/S0012-821X\(99\)00238-1](https://doi.org/10.1016/S0012-821X(99)00238-1)
- Muzellec, T., De Landro, G., Camanni, G., Adinolfi, G.M. and Zollo, A. 2024. The complex 4D multi-segmented rupture of the 2014 Mw 6.2 Northern Nagano Earthquake revealed by high-precision aftershock locations. *ESS Open Archive*, <https://doi.org/10.22541/essoar.171291607.76518097/v1>
- Palo, M., Picozzi, M., De Landro, G. and Zollo, A. 2023a. Microseismicity clustering and mechanic properties reveal fault segmentation in southern Italy. *Tectonophysics*, **856**, <https://doi.org/10.1016/j.tecto.2023.229849>
- Palo, M., Scotto di Uccio, F., Picozzi, M. and Festa, G. 2023b. An Enhanced Catalog of Repeating Earthquakes on the 1980 Irpinia Fault System, Southern Italy. *Geosciences*, **14**, <https://doi.org/10.3390/geosciences14010008>
- Pantosti, D. and Valensise, G. 1990. Faulting mechanism and complexity of the November 23, 1980, Campania–Lucania earthquake, inferred from surface observation. *Journal of Geophysical Research*, **95**, <https://doi.org/10.1029/jb095ib10p15319>
- Patacca, E. 2007. Stratigraphic constraints on the CROP-04 seismic line interpretation: San Fele 1, Monte Foi 1 and San Gregorio Magno 1 wells (southern Apennines, Italy). *Bollettino della Società Geologica Italiana*, **7**, 185–239.
- Patacca, E. and Scandone, P. 2007. Geology of the Southern Apennines. *Bollettino della Società Geologica Italiana*, **7**, 75–119.
- Pescatore, T., Renda, P., Schiattarella, M. and Tramutoli, M. 1999. Stratigraphic and structural relationships between Meso-Cenozoic Lagonegro basin and coeval carbonate platforms in southern Apennines, Italy. *Tectonophysics*, **315**, 269–286, [https://doi.org/10.1016/S0040-1951\(99\)00278-4](https://doi.org/10.1016/S0040-1951(99)00278-4)
- Picozzi, M., Bindi, D., Zollo, A., Festa, G. and Spallarossa, D. 2019. Detecting long-lasting transients of earthquake activity on a fault system by monitoring apparent stress, ground motion and clustering. *Scientific Reports*, **9**, 1–11, <https://doi.org/10.1038/s41598-019-52756-8>
- Pingue, F., De Natale, G. and Briole, P. 1993. Modelling of the 1980 Irpinia earthquake source: constraints from geodetic data. *Annals of Geophysics*, **36**, 27–40, <https://doi.org/10.4401/ag-4296>
- Reasenber, P. and Oppenheimer, D.H. 1985. *FFFIT, FPLOT and FPPAGE; Fortran Computer Programs for Calculating and Displaying Earthquake Fault-Plane Solutions (No. 85-739)*. US Geological Survey.
- RISSC-Lab 2024. *RISSC-Lab Report on the Mw 3.9 Ricigliano Earthquake (Italy, 2024-02-10)*. Zenodo, <https://doi.org/10.5281/zenodo.10657217>
- Roure, F., Casero, P. and Vially, R. 1991. Growth processes and melange formation in the southern Apennines accretionary wedge. *Earth and*

- Planetary Science Letters*, **102**, 395–412, [https://doi.org/10.1016/0012-821X\(91\)90031-C](https://doi.org/10.1016/0012-821X(91)90031-C)
- Schaff, D.P. and Waldhauser, F. 2005. Waveform cross-correlation-based differential travel-time measurements at the Northern California Seismic Network. *Bulletin of the Seismological Society of America*, **95**, 2446–2461, <https://doi.org/10.1785/0120040221>
- Scotto di Uccio, F., Michele, M. *et al.* 2024. Characterization and evolution of seismic sequences in the normal fault environment of the Southern Apennines. *Journal of Geophysical Research: Solid Earth*, **129**, <https://doi.org/10.1029/2023JB028644>
- Shiner, P., Beccacini, A. and Mazzoli, S. 2004. Thin-skinned versus thick-skinned structural models for Apulian carbonate reservoirs: constraints from the Val D'Agri Fields. *Marine and Petroleum Geology*, **21**, 805–827, <https://doi.org/10.1016/j.marpetgeo.2003.11.020>
- Tarantino, S., Poli, P., D'Agostino, N., Vassallo, M., Festa, G., Ventafridda, G. and Zollo, A. 2024. Non-linear elasticity, earthquake triggering and seasonal hydrological forcing along the Irpinia fault, southern Italy. *Nature Communications*, **152**, 9821.
- Tavani, S., Camanni, G. *et al.* 2020. The Mountain Front Flexure in the Lurestan region of the Zagros belt: crustal architecture and role of structural inheritances. *Journal of Structural Geology*, **135**, <https://doi.org/10.1016/j.jsg.2020.104022>
- Waldhauser, F. and Ellsworth, W.L. 2000. A double-difference earthquake location algorithm: method and application to the northern Hayward fault, California. *Bulletin of the Seismological Society of America*, **90**, 1353–1368, <https://doi.org/10.1785/0120000006>
- Wessel, P., Luis, J.F., Uieda, L., Scharroo, R., Wobbe, F., Smith, W.H.F. and Tian, D. 2019. The generic mapping tools version 6. *Geochemistry, Geophysics, Geosystems*, **20**, 5556–5564, <https://doi.org/10.1029/2019GC008515>
- Westaway, R. and Jackson, J. 1984. Surface faulting in the southern Italian Campania–Basilicata earthquake of 23 November 1980. *Nature*, **312**, 436–438, <https://doi.org/10.1038/312436a0>